

---


Electronic Theses and Dissertations, 2004-2019

---

2014

## LP fiber mode converters using holographic phase mask in photo-thermo-refractive glass

Aniket Patil  
*University of Central Florida*

 Part of the [Electromagnetics and Photonics Commons](#), and the [Optics Commons](#)  
Find similar works at: <https://stars.library.ucf.edu/etd>  
University of Central Florida Libraries <http://library.ucf.edu>

This Masters Thesis (Open Access) is brought to you for free and open access by STARS. It has been accepted for inclusion in Electronic Theses and Dissertations, 2004-2019 by an authorized administrator of STARS. For more information, please contact [STARS@ucf.edu](mailto:STARS@ucf.edu).

---

### STARS Citation

Patil, Aniket, "LP fiber mode converters using holographic phase mask in photo-thermo-refractive glass" (2014). *Electronic Theses and Dissertations, 2004-2019*. 4828.  
<https://stars.library.ucf.edu/etd/4828>

LP FIBER MODE CONVERTERS USING HOLOGRAPHIC PHASE MASK IN PHOTO-  
THERMO-REFRACTIVE GLASS

by

ANIKET PATIL  
B.E. Pune University, 2011

A thesis submitted in partial fulfillment of the requirements  
for the degree of Master of Science  
in the Department of Optics  
in the College of Optics and Photonics  
at the University of Central Florida  
Orlando, Florida

Summer Term  
2014

Major Professor: Axel Schulzgen

© 2014 Aniket Patil

## ABSTRACT

In this study, an investigation was undertaken to research the use of holographic phase masks (HPMs) in photo-thermo-refractive (PTR) glass as mode converters for linearly polarized (LP) fiber modes. A Spatial Light Modulator (SLM) was used to generate higher-order transverse fiber modes  $LP_{m,n}$ . Under proper incidence condition on the holographic device,  $LP_{m,n}$  modes are diffracted and simultaneously converted into higher order or lower order LP modes. The process was analyzed by imaging the far field on a CCD camera. It is demonstrated that using this novel method of converting transverse fiber modes several combinations of LP modes can be converted to each other with mode conversion efficiencies up to 70%. Mode purities were found to be around 85% for up conversion and around 90% for down conversion, respectively. It is noticed that this approach has several promising applications such as mode multiplexing, beam cleaning and power scaling of higher-order mode fiber lasers and amplifiers by combining mode conversion and beam combining.

*Dedicated to my parents*

# TABLE OF CONTENTS

LIST OF FIGURES .....	vii
LIST OF TABLES .....	ix
LIST OF ABBREVIATIONS.....	x
CHAPTER 1. INTRODUCTION .....	1
1.1 Motivation and Prior Work.....	1
1.2 Photo-thermo-refractive (PTR) Glass.....	3
CHAPTER 2. OPTICAL DEVICE FOR MODE CONVERSION: HOLOGRAPHIC PHASE MASK.....	5
2.1 Theoretical Approach.....	5
2.2 Presentation of the HPM.....	6
2.2.1 Fabrication Process .....	6
2.2.2 Device Parameters .....	7
CHAPTER 3. EXPERIMENT 1: BROADBAND OPERATION OF HPM .....	9
3.1 Introduction to LP Modes .....	9
3.2 Experimental Setup.....	12
3.3 Broadband Operation Results .....	15
3.3.1 Up Conversion of LP <sub>01</sub> Mode .....	15

3.3.2 Angular Selectivity .....	17
CHAPTER 4. EXPERIMENT 2: LP MODE CONVERSION.....	19
4.1 Generation of LP Modes Using Spatial Light Modulator.....	19
4.2 Experimental Setup for Mode Conversion .....	21
4.3 LP Mode Conversion Results .....	22
4.3.1 Correlations of Converted modes .....	22
4.3.2 Mode Conversion Efficiency .....	29
CHAPTER 5. SUMMARY, CONCLUSION AND OUTLOOK.....	33
APPENDIX. ENCODING LP MODES ON SLM .....	34
REFERENCES .....	37

## LIST OF FIGURES

Figure 1: Absorption spectrum of PTR glass.....	3
Figure 2: Setup to record the HPM.....	6
Figure 3: (a) Four sector phase mask (b) Eight sector phase mask .....	7
Figure 4: Holographic phase mask .....	7
Figure 5: Combination of TE <sub>01</sub> mode with HE <sub>21</sub> mode to generate LP <sub>11</sub> mode.....	9
Figure 6: LP <sub>m,n</sub> modes guided in optical fiber .....	10
Figure 7: Simulated MFAs of LP <sub>m,n</sub> modes for 40 μm core fiber at 1064 nm .....	11
Figure 8 : Experimental setup to verify broadband operation of HPM .....	12
Figure 9: Incident beam position on HPM.....	13
Figure 10 : Spectra of laser sources (a) 638 nm (b) 976 nm (c) 1064 nm .....	14
Figure 11: Up conversion of LP <sub>01</sub> mode into LP <sub>21</sub> mode at 638 nm.....	15
Figure 12 : Up conversion of LP <sub>01</sub> mode into LP <sub>21</sub> mode at 976 nm.....	16
Figure 13 : Up conversion of LP <sub>01</sub> mode into LP <sub>21</sub> mode at 1064 nm.....	17
Figure 14: (a) Far field of converted mode at Bragg angle (b) Far field of converted mode for a 0.5° deflection of HPM from Bragg condition.....	18
Figure 15: Cross section of SLM device.....	19
Figure 16: Schematic of spatial distribution of encoded field spectra.....	20
Figure 17: Experimental setup for mode conversion.....	21
Figure 18: Reference LP modes generated using SLM (a) LP <sub>01</sub> mode (b) LP <sub>11e</sub> mode (c) LP <sub>11o</sub> mode (d) LP <sub>21</sub> mode (e) Image section for LP <sub>11e</sub> mode along maxima .....	23



Figure 19: Up conversion of LP <sub>01</sub> mode in LP <sub>11o</sub> mode.....	25
Figure 20: Up conversion of LP <sub>01</sub> mode in LP <sub>11e</sub> mode.....	25
Figure 21: Up conversion of LP <sub>01</sub> mode in LP <sub>21</sub> mode.....	26
Figure 22: Down conversion of LP <sub>11o</sub> mode in LP <sub>01</sub> mode .....	27
Figure 23: Down conversion of LP <sub>11e</sub> mode in LP <sub>01</sub> mode.....	27
Figure 24: Down conversion of LP <sub>21</sub> mode in LP <sub>01</sub> mode.....	28
Figure 25: Stray mode content left in LP <sub>01</sub> mode down converted from LP <sub>11e</sub> mode .....	29
Figure 26: Calculation of stray mode power.....	30
Figure 27: Field, Phase and Intensity profiles of extracted mode.....	35
Figure 28: (a) Field profile encoded on SLM (b) Corresponding intensity profile .....	36

## LIST OF TABLES

Table 1: Bragg condition for different wavelengths .....	17
Table 2: Mode correlation factor of converted modes .....	28
Table 3: Mode conversion efficiencies of converted modes .....	32

## **LIST OF ABBREVIATIONS**

HOM: Higher Order Mode

HPM: Hologram of Phase Mask

LMA: Large Mode Area

LP: Linearly Polarized

PTR: Photo-Thermo-Refractive

SMF: Single Mode Fiber

SNR: Signal to Noise Ratio

TEM: Transverse Electro-Magnetic

UV: Ultra Violet

VBG: Volume Bragg Graing

# CHAPTER 1. INTRODUCTION

## 1.1 Motivation and Prior Work

Fiber lasers have many advantages of being compact, stable, versatile, cost effective and they deliver extremely good beam quality due to their waveguide structure [1]. Although optical fibers were developed as a low loss propagation media for telecommunication [2], due to their advantages and high power scalability fiber lasers have been of special interest in solid state media laser development [3].

Typical step index fiber designs consist of a simple core and cladding structure, where core has higher refractive index than that of cladding. Light is guided through core by principal of total internal reflection [4]. When doped with rare earth materials, these fiber structures have shown high gain efficiency with diffraction limited beam output [5]. Despite of these advantages typical single mode fibers have some limitations [6]. With increase in power levels, small core size gives rise to high intensity. Due to high intensity these fiber systems suffer from nonlinear effects such as self-phase modulation, stimulated Brillouin scattering and stimulated Raman scattering. These effects affect performance of lasers by limiting output power and unstable laser operations [7], [8], [9]. High intensity in fibers may also cause thermal damage [6].

To tackle these issues the core diameter can be increased. Though increasing core diameter gives rise to multimode operation which in turn degrades beam quality [10] [11]. To get diffraction limited beam output systems with large mode area (LMA) fibers and complex photonic crystal fibers have been designed. These fibers have larger effective mode area with typically single mode guidance [12], [13]. Higher effective area reduces intensity which in turns reduces nonlinear

effects and increases damage threshold. Although for higher power after a certain power limit these systems suffer with mode instabilities [12], [14], [15]. Mode instabilities affect beam quality adversely, effectively negating one of the major advantages of fiber lasers [16].

The goal to achieve power scalability with diffraction limited quality of the beam was motivation behind this thesis. The idea was to use higher order mode (HOM) fiber amplifiers and laser systems. Since higher order mode has higher effective mode area higher power levels can be achieved increasing the onset of nonlinearities [17]. After amplification of HOM, an approach is proposed to efficiently convert HOM back into fundamental mode to get diffraction limited beam quality. The mode converter device used is a Holographic Phase Mask (HPM) in Photo-Thermo-Refractive (PTR) glass.

This investigation covers characterization of HPM for broadband operation, up conversion from fundamental linearly polarized (LP) fiber mode to HOMs and down conversion from HOMs to fundamental LP mode. LP modes are discussed in chapter 3.

Previously Segal, M. et. al. have shown mode conversion using phase mask made in PTR glass for TEM modes [18], [19]. TEM modes are approximate solutions of Maxwell's equation describing propagation of the electric field free space. The electric field distribution of these modes is essentially the product of a Gaussian and a Hermite polynomial [20][21]. For a TEM<sub>m,n</sub> mode, the field distribution is given by,

$$E_{m,n}(x, y, z) = E_0 \frac{w_0}{w(z)} H_m \left( \sqrt{2} \frac{x}{w(z)} \right) \exp \left( -\frac{x^2}{w(z)^2} \right) \cdot H_n \left( \sqrt{2} \frac{y}{w(z)} \right) \exp \left( -\frac{y^2}{w(z)^2} \right) \cdot \exp \left( -i \left( kz - (1 + n + m) \tan^{-1} \left( \frac{z}{z_r} \right) + \frac{k(x^2 + y^2)}{2R(z)} \right) \right) \quad (1)$$

where,  $H_m(x)$  and  $H_n(x)$  are Hermite polynomials with  $m, n \geq 0$ .

This study is organized in five chapters starting with a brief introduction of PTR glass in Chapter 1. In Chapter 2 an overview of HPM is given. The chapter covers theoretical approach, fabrication process and device parameters. The first experiment is presented in Chapter 3 where broadband operation of the HPM device is demonstrated. The chapter gives an overview of the LP modes, details about the experimental setup and the results are discussed. Chapter 4 discusses about a second experiment where conversion between several LP modes combinations is demonstrated. To do so, a spatial light modulator was used and details regarding its operation are provided. Furthermore, experimental results of mode conversion at 1064 nm light wavelength are discussed. Chapter 5 gives a brief summary and conclusion of the study.

### **1.2 Photo-thermo-refractive (PTR) Glass**

PTR glass is used to fabricate volume Bragg gratings (VBG), phase masks, the HPM etc [22], [19]. It is a multicomponent silica glass doped with silver, cerium and fluorine. The glass is photosensitive with photosensitivity higher than traditional Germanium doped glasses. PTR glass has a wide transparency window from 350 to 2700 nm which makes it suitable for IR applications.

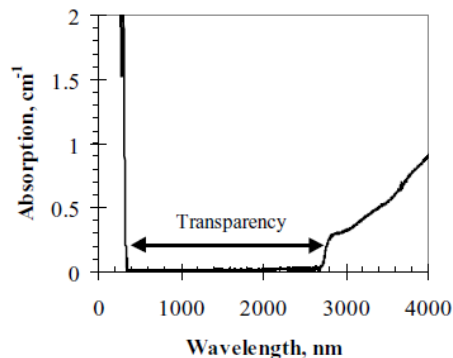


**Figure 1: Absorption spectrum of PTR glass [23]**

PTR glass has high damage threshold of  $10 \text{ J/cm}^2$  for a 1 ns laser pulse. No significant temperature change has been reported under illumination of  $100 \text{ KW/cm}^2$ . these properties make it particularly useful for high power applications [19], [23].

Photosensitivity makes PTR glass special. When the glass is exposed to ultra violet (UV) wavelength from 280 to 350 nm, the cerium ionizes. The electron released by cerium is accepted by silver and it becomes a neutral atom. After exposure to UV radiation the glass is heated. During heating process formations of silver crystals occurs at  $450\text{-}500^\circ \text{ C}$ . These silver crystals act as seed for sodium fluoride crystal growth. Sodium fluoride crystal growth occurs between  $500$  to  $550^\circ \text{ C}$ . This process of exposure to UV radiation and heating is known as photo-thermo process. After Photo-thermo process permanent refractive index change of  $10^{-3}$  order occurs. The change in refractive index is permanent unless the glass is heated above  $400^\circ \text{ C}$  [23].

## CHAPTER 2. OPTICAL DEVICE FOR MODE CONVERSION: HOLOGRAPHIC PHASE MASK

The mode converter device used is a holographic phase mask (HPM) recorded in PTR glass. This chapter discusses about the theoretical approach, fabrication method and device parameters of HPM.

### 2.1 Theoretical Approach

The HPM is a phase mask encoded in tilted transmitting volume Bragg grating (VBG) and it is important to understand the propagation of light through this holographic device. VBGs were numerically modeled by H. Kogelnik. The model is known as coupled wave theory [24], [25]. The numerical model used HPM was developed by Segal, M. et.al using coupled wave theory [18]. For convenience it was assumed that the incident beam exactly satisfies Bragg condition. Under this condition coupled wave equations become

$$\frac{1}{k_i} \left( k_{i,x} \frac{\delta A}{\delta x} + k_{i,y} \frac{\delta A}{\delta y} + k_{i,z} \frac{\delta A}{\delta z} \right) = -i\kappa e^{-i\varphi(x,y)} B \quad (2)$$

$$\frac{1}{k_i} \left( k_{d,x} \frac{\delta A}{\delta x} + k_{d,y} \frac{\delta A}{\delta y} + k_{d,z} \frac{\delta A}{\delta z} \right) = -i\kappa e^{-i\varphi(x,y)} A \quad (3)$$

$\kappa = \pi n/\lambda_0$ ,  $\lambda_0$  is free space wavelength,  $A$  and  $B$  are complex amplitudes of transmitted and diffracted waves respectively,  $k_i$  is wavenumber of incident beam and  $k_d$  is wavenumber of diffracted beam. Now converting equation 2 and 3 in Fourier domain along transverse axes (x and y axes) we get,

$$\frac{2\pi i}{k_i} (f_x k_{i,x} + f_y k_{i,y}) \tilde{A} + \frac{k_{i,z}}{k_i} \frac{\delta \tilde{A}}{\delta z} = F(-i\kappa e^{-i\varphi(x,y)} B) \quad (4)$$

$$\frac{2\pi i}{k_i} (f_x k_{d,x} + f_y k_{d,y}) \tilde{B} + \frac{k_{d,z}}{k_i} \frac{\delta \tilde{B}}{\delta z} = F(-i\kappa e^{-i\varphi(x,y)} A) \quad (5)$$



Where  $\tilde{A}$  and  $\tilde{B}$  are Fourier transforms of  $A$  and  $B$  respectively. Assuming small propagation steps ( $\Delta z$ ) right hand side of the equations 4 and 5 becomes approximately zero. Taking inverse Fourier transform amplitude in real space is

$$A(x, y, z + \Delta z) = F^{-1} \left( \tilde{A}(f_x, f_y, z + \Delta z) \right) - i\kappa e^{-i\varphi(x,y)} B(x, y, z) \Delta z \quad (6)$$

$$A(x, y, z + \Delta z) = F^{-1} \left( \tilde{A}(f_x, f_y, z + \Delta z) \right) - i\kappa e^{-i\varphi(x,y)} B(x, y, z) \Delta z \quad (7)$$

Calculations using this numerical model indicate that for a short step size of 100 nm energy is conserved within 0.01%. Thus in theory the propagation through entire system is extremely efficient with almost 100% transmission [18].

## 2.2 Presentation of the HPM

### 2.2.1 Fabrication Process

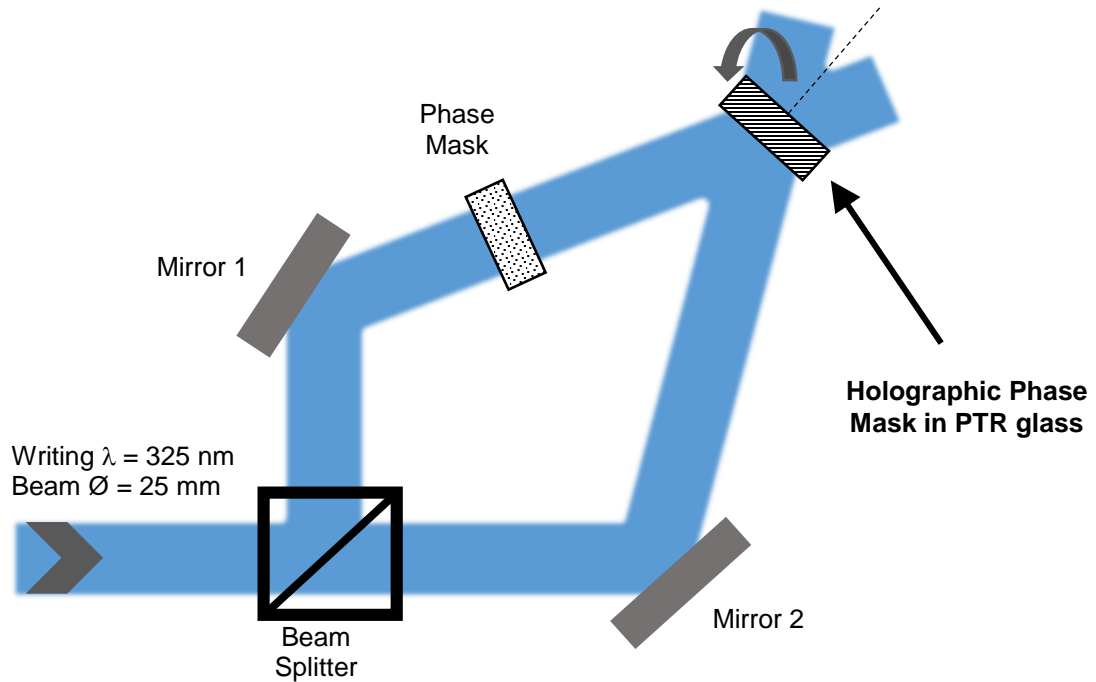


**Figure 2: Setup to record the HPM**

A two beam interference setup was used to fabricate the HPM. Figure 2 shows the schematic of the setup used to record the holographic device. A phase mask was kept in one arm of the interferometer. Fringe period for recording was controlled by mirror tilt. The recording wavelength used was 325 nm with a beam diameter of 25 mm. A four sector phase mask as shown in figure 3(a) was used to record the holographic device. Even though different types of phase masks as shown in figure 3(b) can also be used to record hologram.

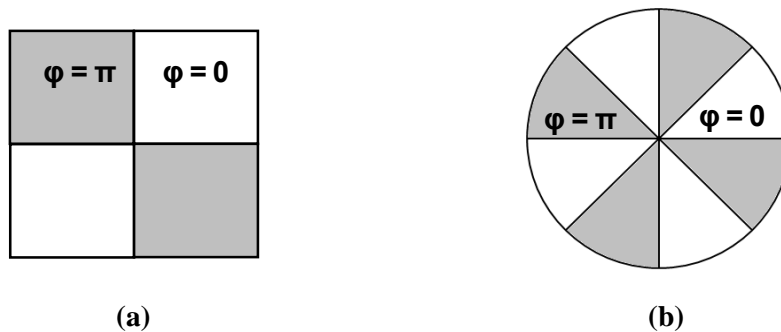


**Figure 3: (a) Four sector phase mask (b) Eight sector phase mask**

### 2.2.2 Device Parameters

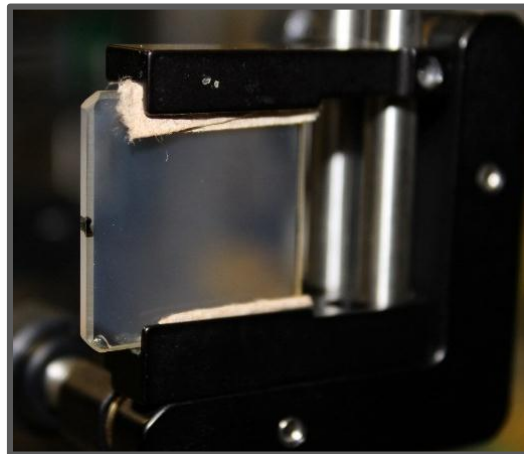


**Figure 4: Holographic phase mask**

The fabricated HPM device is shown in figure 4. The device has a grating period of  $10\ \mu\text{m}$  with a refractive index modulation of 250 ppm. Size of HPM is  $2.5\ \text{cm} \times 2.5\ \text{cm}$  with thickness of 2 mm. The device has high angular selectivity and operates over a broad range of wavelengths [18].

## CHAPTER 3. EXPERIMENT 1: BROADBAND OPERATION OF HPM

In this experiment, fundamental LP mode ( $LP_{01}$ ) was excited in a single mode fiber at three different wavelengths 638 nm, 976 nm and 1064 nm respectively. The  $LP_{01}$  mode was then up converted to  $LP_{21}$  under proper incident condition on the HPM for each wavelength. This experiment serves as a proof that the holographic mode converter device can operate over a broad range of wavelengths.

### 3.1 Introduction to LP Modes

In an optical fiber, guided modes in core are solution of Bessel function of first kind and cladding modes are solution of modified Bessel function of second kind [26]. Typical optical fibers satisfy the paraxial approximation where the index contrast between core and cladding is very small. In such case, it can be assumed that the fiber is weakly guiding. When solved under this approximation, solutions of the wave equation, called transvers modes ( $TE_{lm}$ ,  $TM_{lm}$ ,  $HE_{lm}$  and  $EH_{lm}$ ) are degenerated i.e. their propagation constants are identical. Thus LP modes are introduced as the linear combination of degenerated modes [4] [10]. For example, combination of  $TE_{01}$  mode with  $HE_{21}$  mode. Under weak guidance approximation, these modes can be combined together to generate  $LP_{11}$  mode as shown in figure 5.

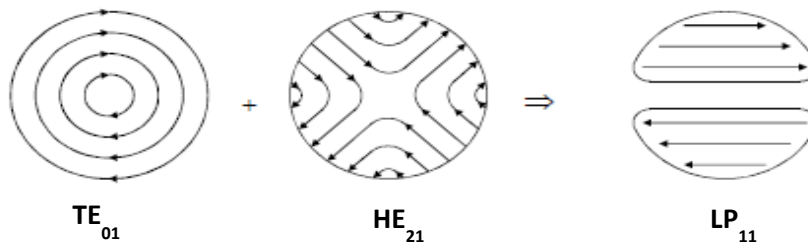


**Figure 5: Combination of  $TE_{01}$  mode with  $HE_{21}$  mode to generate  $LP_{11}$  mode [10]**

LP modes are denoted as  $LP_{m,n}$ , where  $m$  is number zeroes in azimuthal direction and  $n$  is number of zeroes + 1 in radial direction. The fundamental LP mode, labelled as has an intensity profile similar to that of Gaussian profile [4]. Other modes are called higher order modes (HOMs). Intensity profiles of few  $LP_{m,n}$  modes are shown in figure 6.

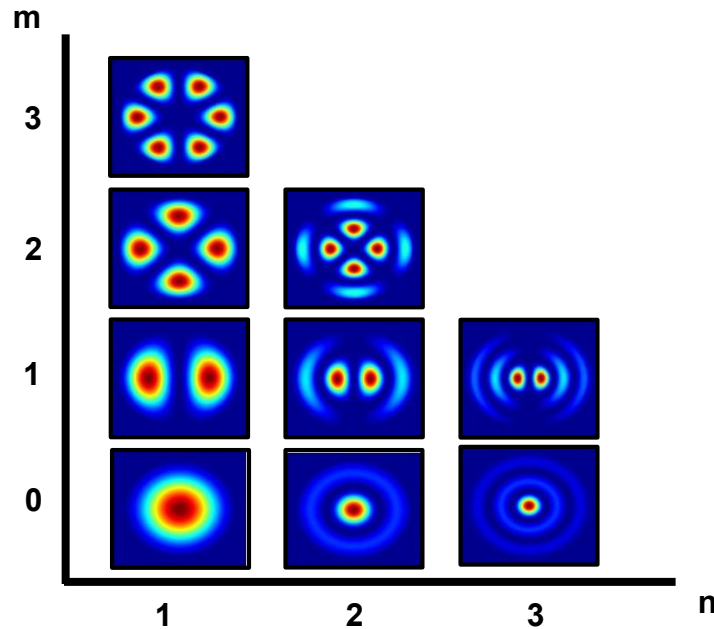


Figure 6:  $LP_{m,n}$  modes guided in optical fiber

An optical fiber which supports only fundamental LP mode and does not support HOMs is known as single mode optical fiber (SMF) [4]. V-number is used to determine if the fiber operates in single mode regime. Equation (8) defines V-number.

$$V = \frac{2\pi}{\lambda} a \sqrt{n_g^2 - n_c^2} \quad (8)$$

where,  $\lambda$  is wavelength of light,  $a$  is radius of the core,  $n_g$  is refractive index of core and  $n_c$  is refractive index of cladding. For  $V < 2.405$  optical fiber operates in single mode regime. Single mode operation is important in fiber laser systems as the far-field profile of the Gaussian beam

emerging the fiber is diffraction limited. Though as explained in chapter 1 these systems suffer from non-linear effects at higher power due to small core size giving rise to high intensity. The way to mitigate non-linear effects is to increase mode field area (MFA). MFA is defined in equation (9) [27].

$$MFA = \frac{2\pi \left[ \int_0^\infty (E(r))^2 r dr \right]^2}{\left[ \int_0^\infty (E(r))^4 r dr \right]} \quad (9)$$

Figure 7 shows calculated MFAs of  $LP_{m,n}$  modes for an optical fiber with 40  $\mu\text{m}$  core diameter at 1064 nm light wavelength. It can be seen from the figure that HOMs have higher MFAs than fundamental mode. It means HOM fiber amplifier and laser systems can be used to achieve better power scalability while reducing the nonlinearities [17]. The motivation of this investigation came from the need to convert these HOM into fundamental mode efficiently with high mode purity to get diffraction limited output beam quality.

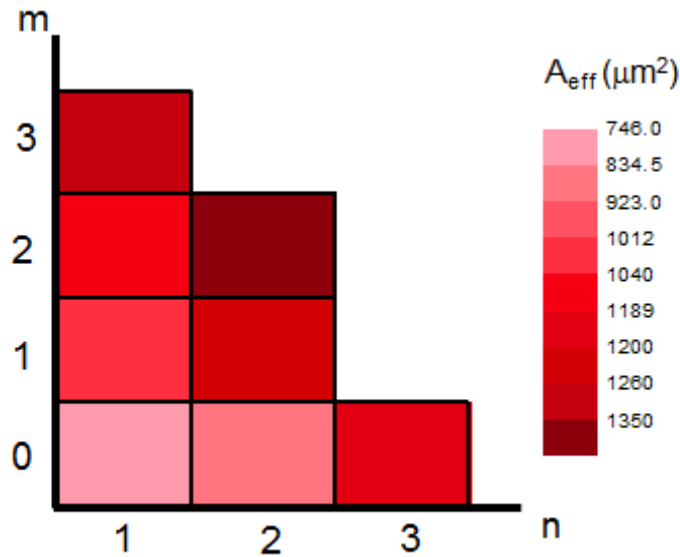


**Figure 7: Simulated MFAs of  $LP_{m,n}$  modes for 40  $\mu\text{m}$  core fiber at 1064 nm**

### 3.2 Experimental Setup

Figure 8 shows experimental setup to verify broadband operation of HPM. A laser source was coupled in single mode fiber held on a X-Y-Z translation stage. The output end of fiber was secured in the holder. A 4x objective was then used to magnify and collimate the output of the fiber. This arrangement was necessary to minimize the effect of external perturbations on output tip of the fiber and keep the distance between fiber tip and collimating objective constant.

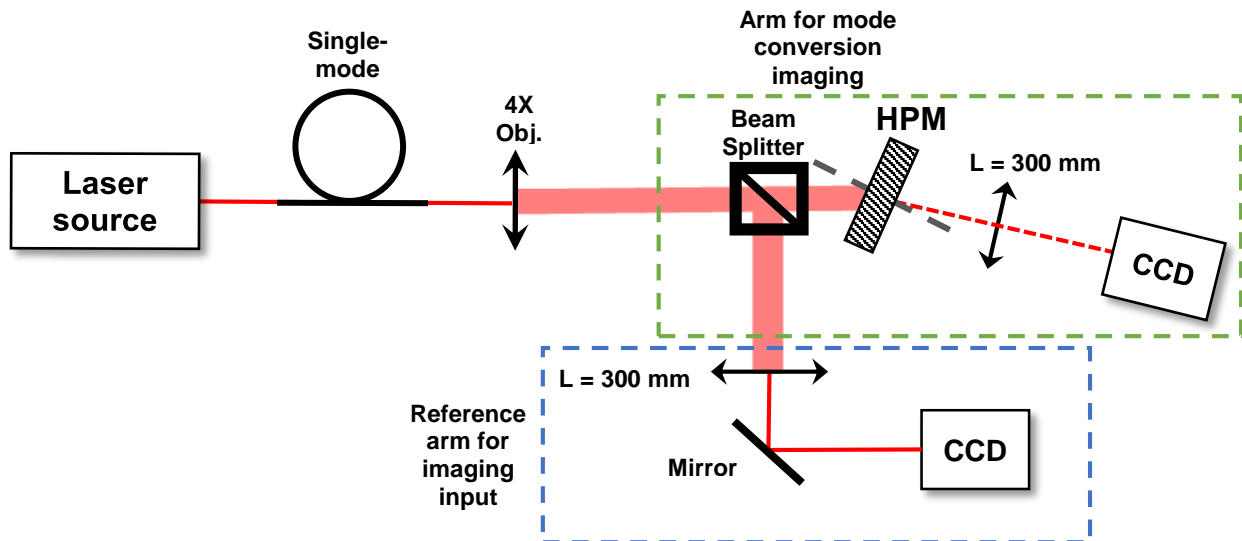


**Figure 8 : Experimental setup to verify broadband operation of HPM**

The constant distance between fiber tip and objective ensured that the collimation of the beam will not change throughout the setup. The collimated beam was then split in two arms using a 50:50 beam splitter, one arm was used as reference arm and other arm was used for mode conversion. The reference arm was used to monitor the input to the HPM. In other arm the beam was incident on HPM at the intersection of four phase sectors. HPM was mounted on a X-Y-Z translation stage

with rotation and tilt abilities. The ability to control all these positions made sure that beam was incident on HPM on the exact position needed. When Bragg condition was met  $LP_{01}$  mode was up converted from to  $LP_{21}$  mode. The incident position of the beam is shown in figure 9.

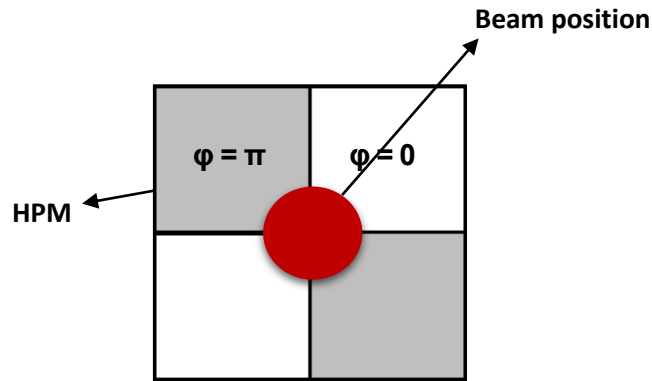


**Figure 9: Incident beam position on HPM**

A convex lens of focal length 300 mm was used to image far field of the converted mode. A camera was then kept at focal point of the lens to image the far field. The camera used for imaging was a CCD camera with sensor size of 1624 pixels  $\times$  1224 pixels. Each pixel is 4.4  $\mu$ m wide [28]. The images captured on camera were stored on a computer and processed in MATLAB. The images were stored in form of a 1624 $\times$ 1224 weighted matrix (same as number of pixels on camera chip). The weight assigned to each matrix element depends on intensity on the respective pixel (higher intensity has higher weight). After storing images in matrix form, the images were normalized and cropped around measured beam. These cropped images were used for further calculations.



A similar imaging arrangement was used in the reference arm as shown in figure 8. Using a similar convex lens of focal length 300 mm, far field of input to the HPM was imaged on CCD camera. Having the reference arm in the setup has provided with ability to monitor input and output of HPM at the same time. This was crucial since it meant the HPM alignment will not be disturbed once Bragg condition was met.

Three laser sources with wavelength 638 nm, 976 nm and 1064 nm were used to verify broadband operation of HPM. Spectra of these sources are shown in figure 10.

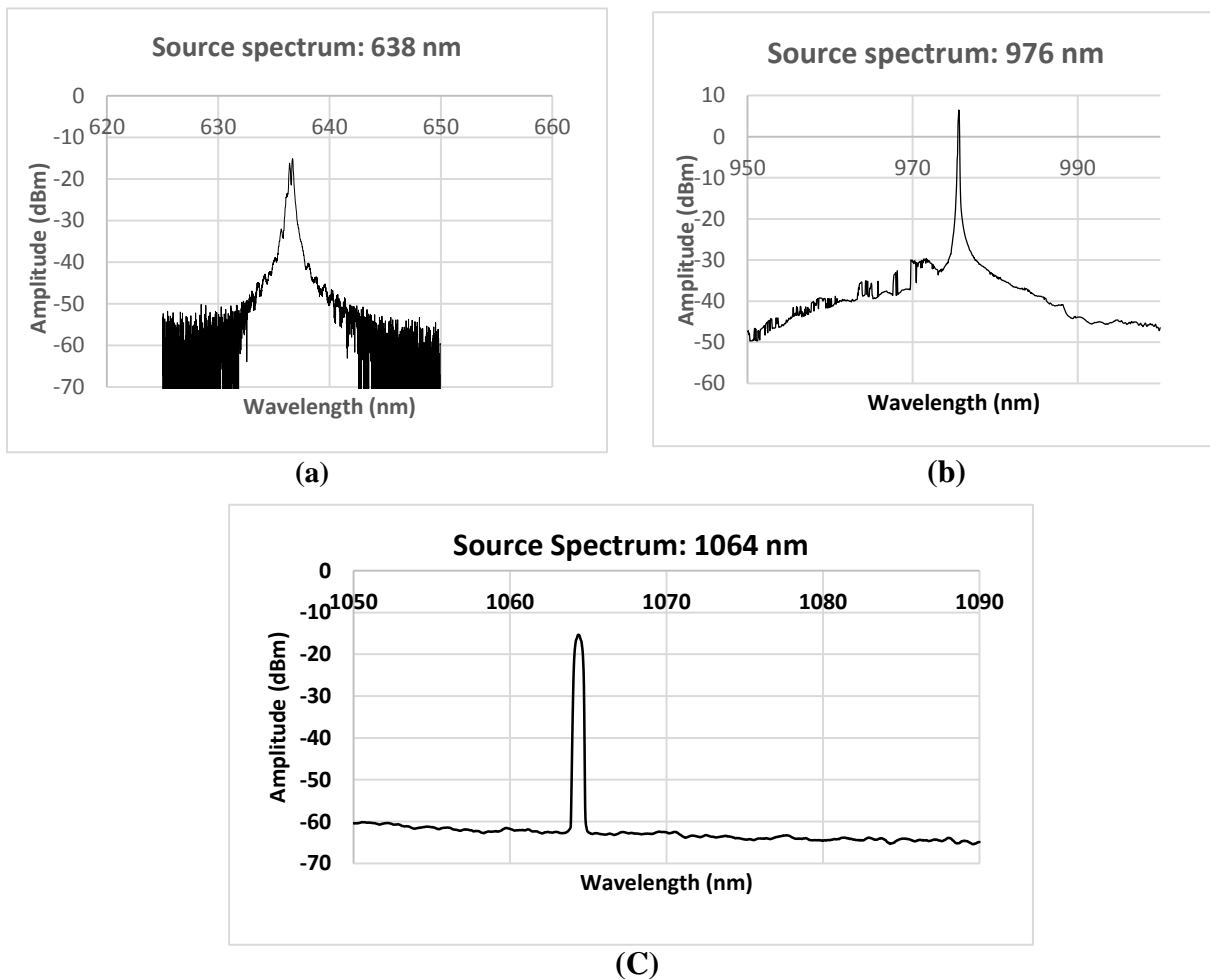


Figure 10 : Spectra of laser sources (a) 638 nm (b) 976 nm (c) 1064 nm

The Laser source was coupled to input end of a single mode fiber while the other (output) end remained fixed on the translation stage as explained, so that there won't be major changes in collimation and only small adjustments were needed to optimize collimation even though the source was changed. Once system was aligned the input to HPM and far field of the converted mode was imaged on camera. The images of far fields were then stored in a computer.

### **3.3 Broadband Operation Results**

The output of single mode fiber ( $LP_{01}$  mode) was collimated and was incident on HPM. Once the collimated beam was positioned at four sector intersection on HPM and Bragg condition was met, up conversion of  $LP_{01}$  into  $LP_{21}$  mode was observed. The experiment was done at 3 different wavelengths 638 nm, 976 nm and 1064 nm as discussed earlier.

#### **3.3.1 Up Conversion of $LP_{01}$ Mode**

##### **3.3.1.1: 638 nm**

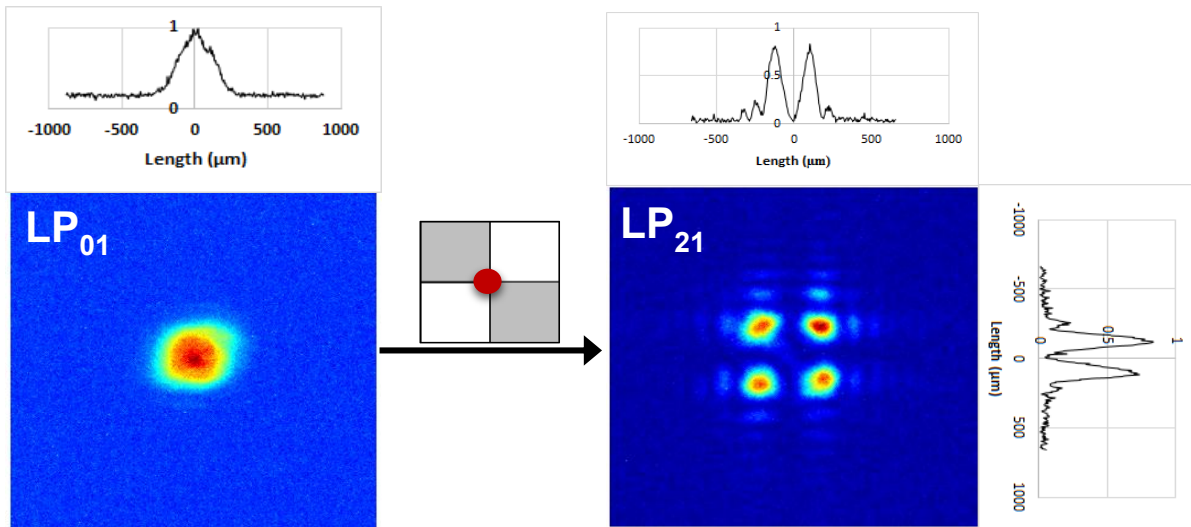


**Figure 11: Up conversion of  $LP_{01}$  mode into  $LP_{21}$  mode at 638 nm**

When incident on HPM under Bragg condition, the  $LP_{01}$  mode was simultaneously diffracted and converted in  $LP_{21}$  mode. Figure 11 shows up conversion of  $LP_{01}$  mode into  $LP_{21}$  mode at 638 nm. The cross section of image through horizontal and vertical axes is shown next to the intensity profile of far field image. It can be clearly seen that the intensity becomes almost zero between two maxima.

### 3.3.1.2: 976 nm

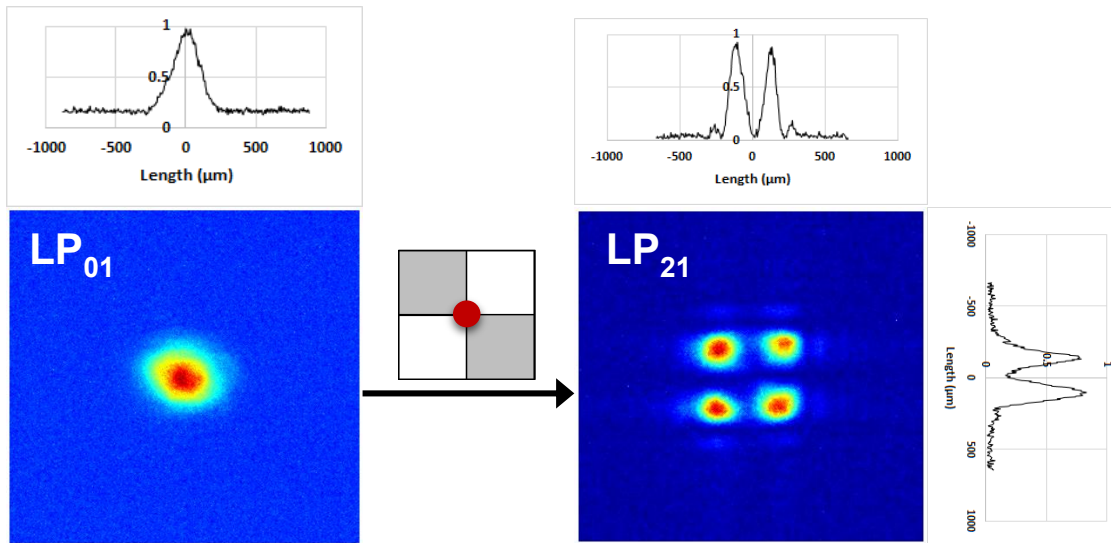


**Figure 12 : Up conversion of  $LP_{01}$  mode into  $LP_{21}$  mode at 976 nm**

$LP_{01}$  mode was converted in  $LP_{21}$  mode at 976 nm. Figure 12 shows up conversion of  $LP_{01}$  at 976 nm.

### 3.3.1.3: 1064 nm

Figure 13 shows up conversion of LP<sub>01</sub> at 1064 nm. LP<sub>01</sub> mode was converted in LP<sub>21</sub> mode at 1064 nm.

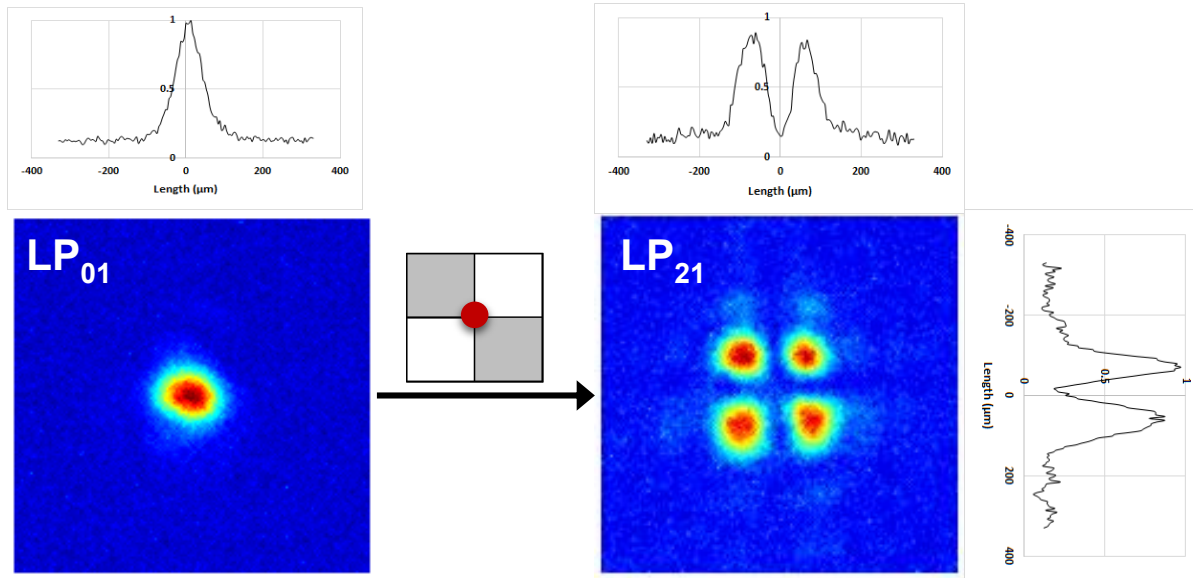


**Figure 13 : Up conversion of LP<sub>01</sub> mode into LP<sub>21</sub> mode at 1064 nm**

### 3.3.2 Angular Selectivity

The HPM is extremely sensitive to angular movement. Maximum diffraction intensity occurs at Bragg condition. Table 1 gives value of calculated incident angle to satisfy Bragg condition at different wavelengths.

**Table 1: Bragg condition for different wavelengths.  $\theta_b$  is incident angle with respect to normal to the surface of the HPM**

Wavelength	$\theta_b$
638 nm	$7.9^0$
976 nm	$7.6^0$
1064 nm	$6.7^0$

It was observed that a slight angular deflection from Bragg condition caused to drop intensity dramatically. Figure 14 shows drop in intensity for a  $0.5^\circ$  change from Bragg angle at 1064 nm. It can be seen from figure that such small deflection causes intensity of the far field to drop down to almost 40% of the intensity of converted mode at Bragg condition. This shows that the HPM has high angular selectivity.

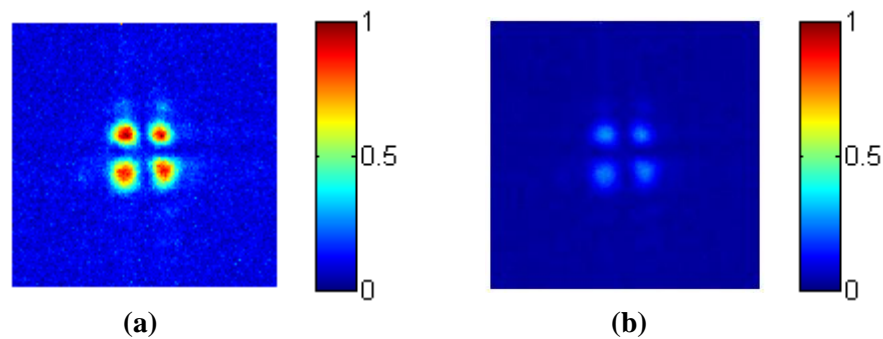


**Figure 14: (a) Far field of converted mode at Bragg angle (b) Far field of converted mode for a  $0.5^\circ$  deflection of HPM from Bragg condition**

The operation of HPM at three different wavelength (638 nm, 976 nm and 1064 nm) verifies that the HPM can be operated over a wide range of wavelengths. The experiment also verifies that the holographic device has high angular selectivity as shown in previous studies [18].

## CHAPTER 4. EXPERIMENT 2: LP MODE CONVERSION

In this experiment LP modes were created using a spatial light modulator (SLM). Under appropriate incidence condition on HPM the fundamental LP mode ( $LP_{01}$ ) was up converted in higher order mode and higher order modes were down converted in fundamental LP mode. In this experiment the mode conversion efficiency and mode correlation of the converted modes was also investigated.

### 4.1 Generation of LP Modes Using Spatial Light Modulator

A Spatial Light Modulator (SLM) from Boulder Nonlinear Systems was used to generate different LP modes. SLM is a device that modulates a coherent beam of light spatially [29]. The device consists of pixels of electrodes with liquid crystals sandwiched between cover glass and electrodes. After a pattern is encoded on SLM, the liquid crystals are aligned according to the electric field. When a monochromatic beam of light is incident on SLM, the liquid crystals modulate complex amplitude of the reflected beam. The reflected beam is then split in multiple diffracted orders with spatial modulation. The required modulated diffraction order (first order of diffraction) is then isolated from the rest of the diffraction orders by spatial filtering (using an iris).

Cross section of SLM is shown in figure 15.

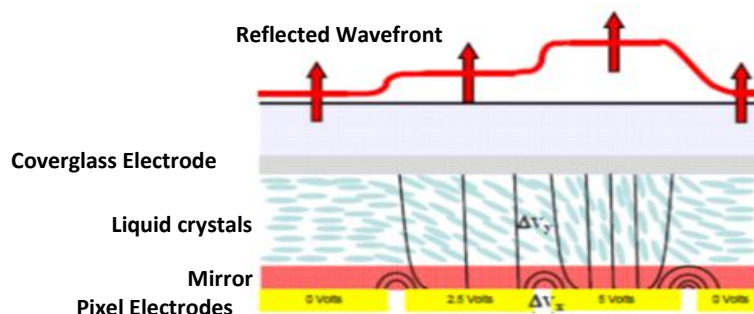


**Figure 15: Cross section of SLM device [30]**

The liquid crystal array size of the device is  $7.68 \times 7.68$  mm with pixel size  $15 \mu\text{m}$ . The pixel array size is  $512 \times 512$  and total number of active pixels is 262,144 [30]. As mentioned earlier, in this experiment SLM was used to modulate complex amplitude of the incident light. Modelling of this technique was done by Arizon, V. et. al [31]. For a complex input field  $s(x,y)$ , the encoded field is given by equation 10

$$h(x, y) = \sum_{q=-\infty}^{\infty} h_q(x, y) \quad (10)$$

where,  $h_q(x, y)$  is  $q^{\text{th}}$  diffraction order. At this point all the diffraction orders are at the same spatial point  $(x, y)$ . This causes a low Signal to Noise Ratio (SNR) because noise from higher orders of diffraction interfering with encoded field in first order of diffraction. To improve the SNR the encoded field is modulated with a carrier signal of phase  $2\pi(u_0x + v_0y)$

$$h_c(x, y) = \sum_{q=-\infty}^{\infty} h_q(x, y) \exp(i2\pi(qu_0x + qv_0y)) \quad (11)$$

The Fourier spectrum of this carrier modulated field is given as

$$H_c(u, v) = \sum_{q=-\infty}^{\infty} H_q(u - qu_0, v - qv_0) \quad (12)$$

This field now has  $0^{\text{th}}$  order at the center and other diffraction orders separated diagonally as shown in figure 16. For this study first order of diffraction ( $q=1$ ) was used because of highest SNR.

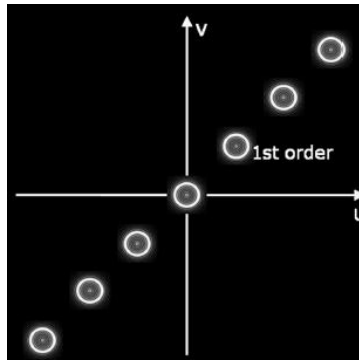


**Figure 16: Schematic of spatial distribution of encoded field spectra [31]**

To encode on SLM, LP modes were generated using a CAD tool FIMMWAVE. FIMMWAVE is a mode solving tool and it can calculate modes of different types of waveguides like standard optical fibers, photonic crystal fibers etc. The calculated modes were then extracted and were encoded on SLM with help of MATLAB. Encoding of these modes on SLM is given in Appendix.

#### 4.2 Experimental Setup for Mode Conversion

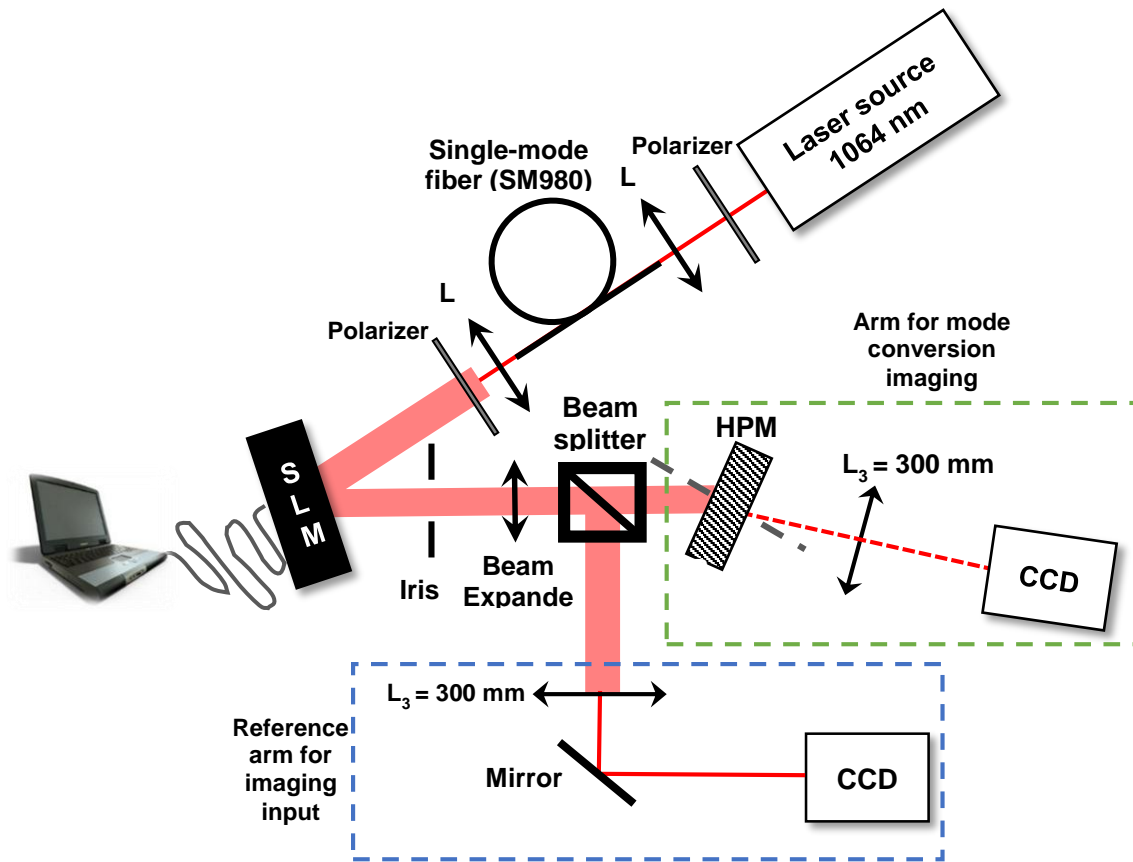


**Figure 17: Experimental setup for mode conversion**

The schematic of experimental setup is shown in figure 17. The light from a 1064 nm laser source was coupled in a SMF, SM980. A lens with focal length 6.5 mm was then used to collimate



the output of the SMF. Two polarizers were used before and after single mode fiber to control the polarization of light incident on SLM. The collimated beam was incident on SLM and was modulated with help of a computer. The modulated beam was encoded in the first order of diffraction. An iris was used to spatially isolate the modulated beam which was then expanded using a beam expander so the beam will be big enough (~4 mm diameter) to be used for mode conversion using the HPM. A beam splitter was used to split the expanded beam in two arms. Similar to the description in section 3.2, one arm was used for mode conversion and other arm was used to image input. The HPM setup and imaging system was same like that was discussed in chapter 3. HPM was mounted on a X-Y-Z translation stage with rotate and tilt abilities. A lens with 300 mm focal length was used to image far field of the converted mode. A similar lens was used to image far field of input to the HPM. The far field was imaged on CCD camera. Camera specifications and details of imaging system are given in chapter 3.

### **4.3 LP Mode Conversion Results**

LP modes generated using SLM were incident on different sectors on the HPM. When appropriate incidence conditions were met, LP modes were converted into each other.

#### **4.3.1 Correlations of Converted modes**

LP modes generated from SLM were considered as reference modes. These modes are shown in figure 18. As it can be seen from the figure 18 (b) and figure 18 (d) there is some distortion in  $LP_{11e}$  and  $LP_{21}$  mode. This distortion arises because of presence of some residual field from zeroth order and higher orders of diffraction in encoded beam even after use of an iris as a spatial filter.

The reference modes were then incident on HPM device and were then converted to higher order or lower order LP modes. In order to evaluate the mode correlation factor, the converted modes were correlated with reference modes (shown in figure 18 (a) to (d)) using MATLAB. The correlation factor serves as measure of similarity between reference as well as converted mode.

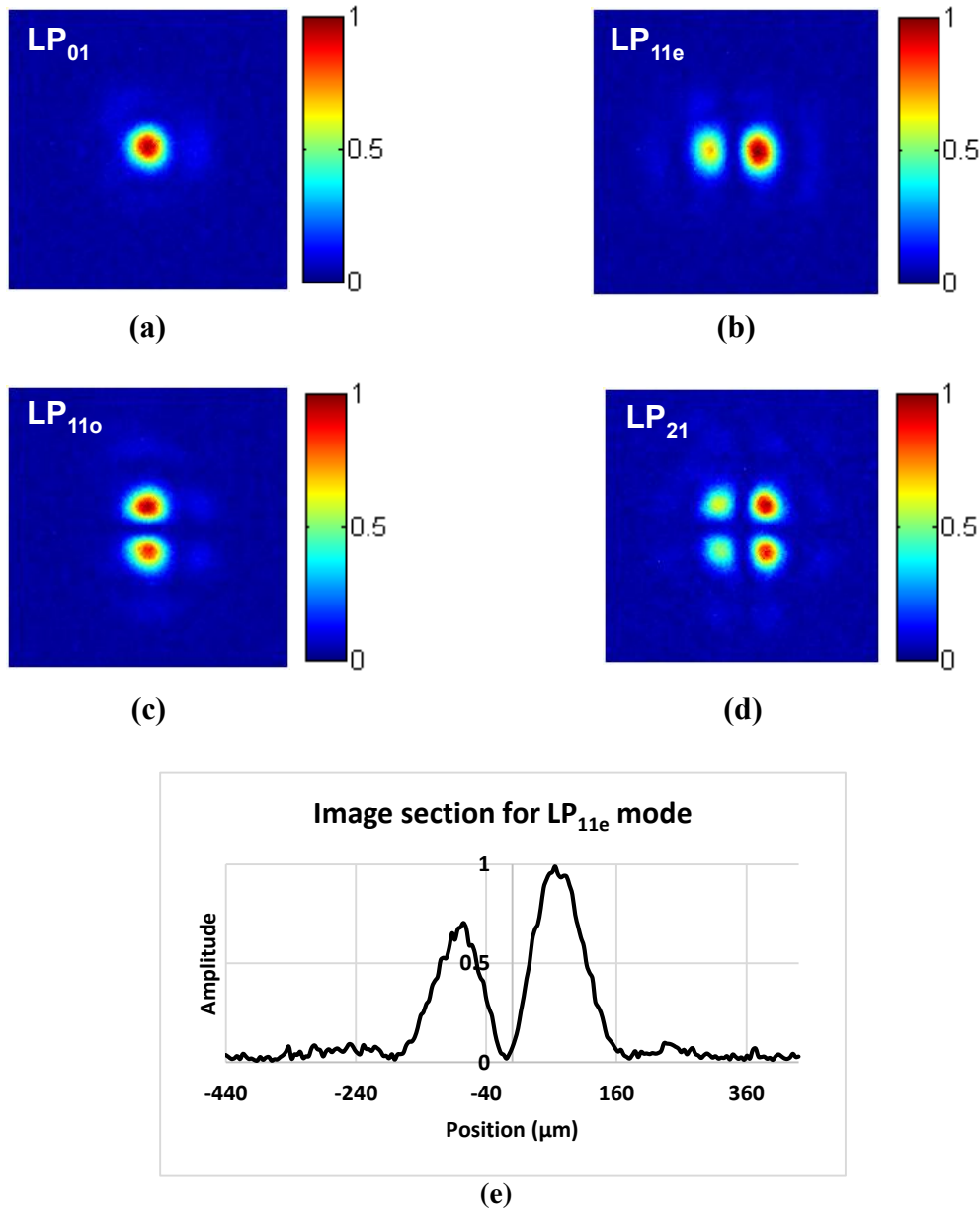


**Figure 18: Reference LP modes generated using SLM (a) LP<sub>01</sub> mode (b) LP<sub>11e</sub> mode (c) LP<sub>11o</sub> mode (d) LP<sub>21</sub> mode (e) Image section for LP<sub>11e</sub> mode along maxima (along horizontal plane)**

As explained earlier in chapter 3, captured images of reference modes and converted modes were stored in a normalized weighted matrix. These image matrices were then used to find the correlation factor between reference and converted modes. The correlation algorithm used in MATLAB is one to one correlation. It means that each element of image matrix is correlated with corresponding element in reference image matrix. That is why it is very important that the both matrices are of same size and modes are well centered in the image. Equation 13 shows the correlation algorithm used

$$\frac{\sum_m \sum_n (A_{m,n} - \bar{A})(B_{m,n} - \bar{B})}{(\sum_m \sum_n (A_{m,n} - \bar{A})^2)(\sum_m \sum_n (B_{m,n} - \bar{B})^2)} \quad (13)$$

where,  $A_{m,n}$  and  $B_{m,n}$  are image matrices of reference and converted mode respectively,  $\bar{A}$  is mean of  $A_{m,n}$  and  $\bar{B}$  is mean of  $B_{m,n}$ .

In 2D correlation, whole image matrix is correlated with reference image matrix. As explained earlier, the correlation factor gives measure of mode similarity.

#### 4.3.1.1. Up Conversion of LP<sub>01</sub> Mode in LP<sub>110</sub> Mode

For up conversion LP<sub>01</sub> mode from SLM (as shown in figure 18 (a)) was incident on HPM and was up converted in LP<sub>110</sub> mode under Bragg condition as shown in figure 19. The section of beam is shown next to the intensity profile. It can be seen from the figure that intensity between two maxima almost drops to zero. The position of beam on HPM is also shown.

Correlation of converted mode was done with reference mode shown in figure 18 (c). The correlation factor was 92%.

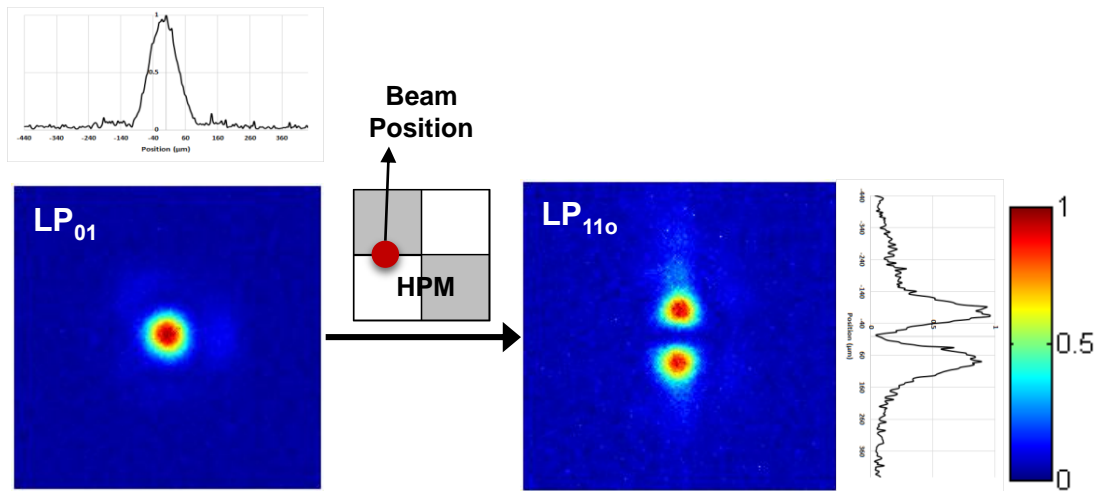


Figure 19: Up conversion of  $LP_{01}$  mode in  $LP_{11o}$  mode.

#### 4.3.1.2. Up conversion of $LP_{01}$ mode in $LP_{11e}$ mode

Up conversion of  $LP_{01}$  mode in  $LP_{11e}$  mode is shown in figure 20. The section of image along maxima is shown next to intensity profile.

When correlated with reference  $LP_{11e}$  mode shown in figure 18 (b), 87% mode correlation was obtained.

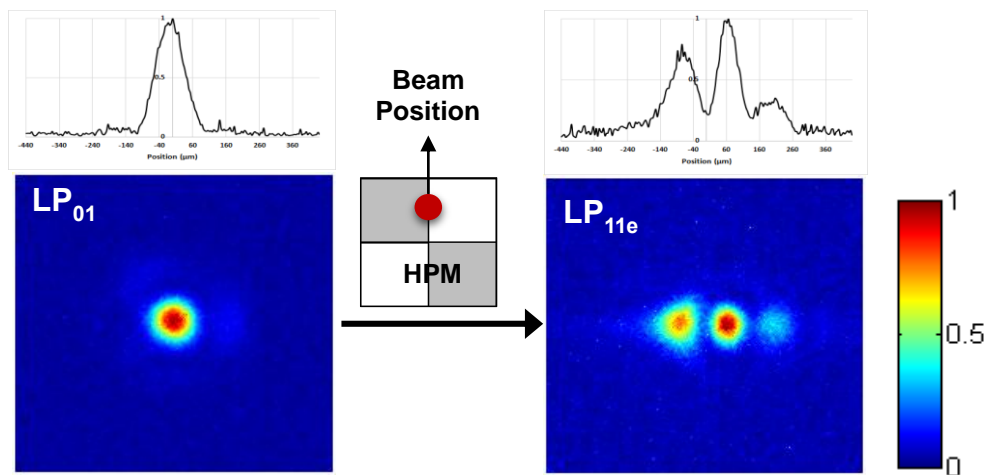
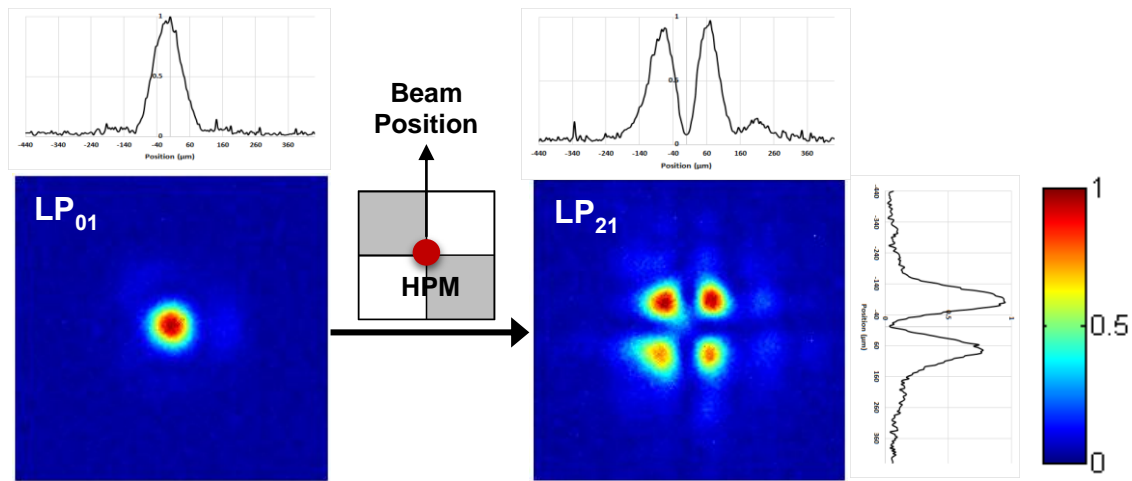


Figure 20: Up conversion of  $LP_{01}$  mode in  $LP_{11e}$  mode.

#### 4.3.1.3. Up conversion of LP<sub>01</sub> to LP<sub>21</sub> mode

Up conversion of LP<sub>01</sub> mode in LP<sub>21</sub> mode is shown in figure 21 with image sections next to intensity profile.



**Figure 21: Up conversion of LP<sub>01</sub> mode in LP<sub>21</sub> mode**

The correlation of converted mode with reference image shown in figure 18 (d) resulted in mode correlation of 82.5%.

#### 4.3.1.4. Down conversion of LP<sub>110</sub> mode in LP<sub>01</sub> mode

For down conversion from LP<sub>110</sub> mode in LP<sub>01</sub> mode, LP<sub>110</sub> mode from SLM as shown in figure 18 (c) was used. When incident on HPM under Bragg condition it was down converted in LP<sub>01</sub> mode as shown in figure 22.

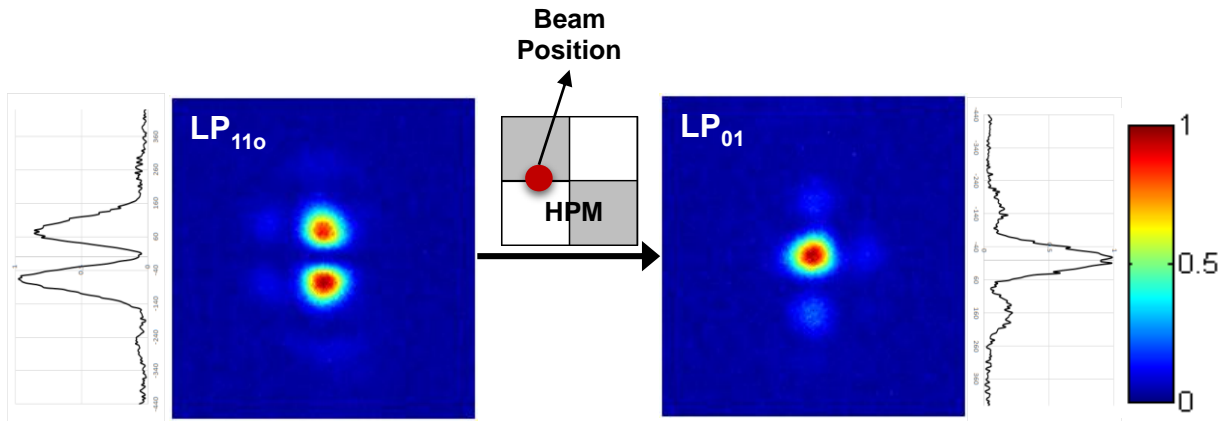


**Figure 22: Down conversion of LP<sub>11o</sub> mode in LP<sub>01</sub> mode**

The converted LP<sub>01</sub> mode was then correlated with reference LP<sub>01</sub> mode as shown in figure 18 (a). For 2D correlation was 91%.

#### 4.3.1.5. Down conversion of LP<sub>11e</sub> mode in LP<sub>01</sub> mode

Down conversion of LP<sub>11o</sub> mode to LP<sub>01</sub> mode is shown in figure 23. Reference LP<sub>11o</sub> mode shown in figure 18 (c) is used as input to HPM.

Converted LP<sub>01</sub> is correlated with reference LP<sub>01</sub> mode shown in figure 18 (a). Mode correlation was 86%.

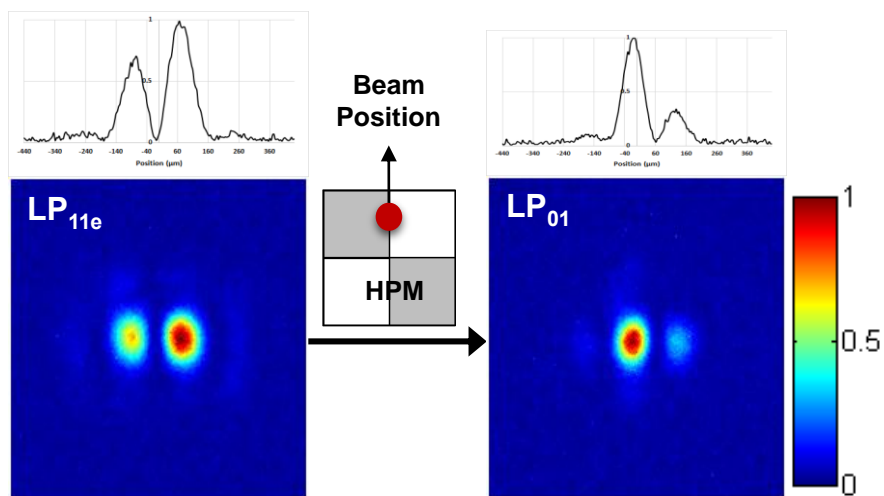


**Figure 23: Down conversion of LP<sub>11e</sub> mode in LP<sub>01</sub> mode**

#### 4.3.1.6. Down conversion of LP<sub>21</sub> mode in LP<sub>01</sub> mode

For down conversion from LP<sub>21</sub> mode into LP<sub>01</sub> mode, LP<sub>21</sub> mode from SLM (shown in figure 18 (d)) was used as input. The down conversion is shown in figure 24.

When correlated with reference LP<sub>01</sub> mode (shown in figure 18 (a)), mode correlation was 91%.

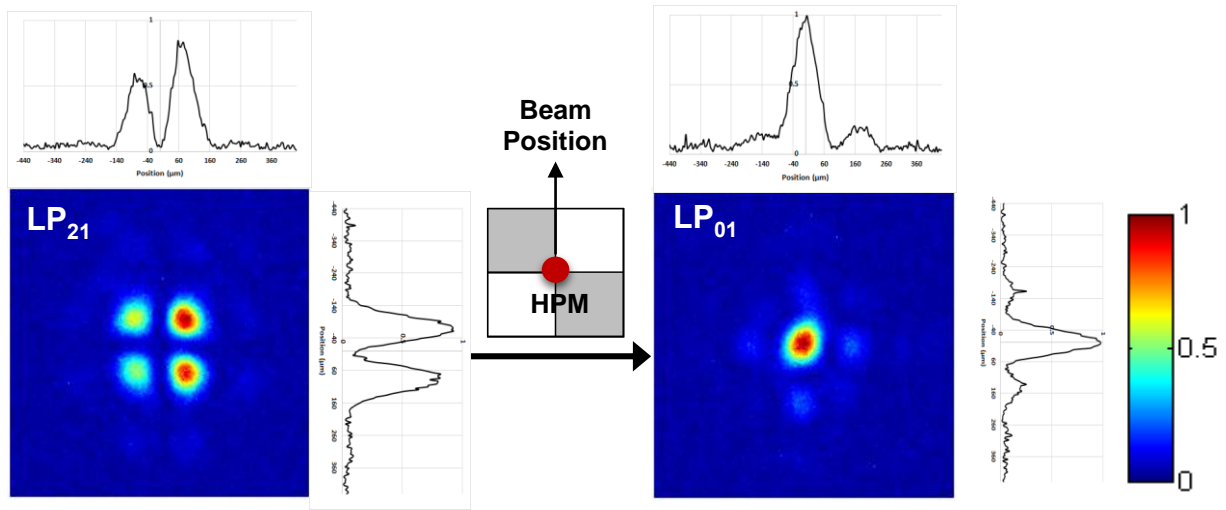


**Figure 24: Down conversion of LP<sub>21</sub> mode in LP<sub>01</sub> mode**

Mode correlation factors for different LP mode conversion are tabulated in table 2.

**Table 2: Mode correlation factor of converted modes**

Input Mode	Converted Mode	Mode correlation
LP <sub>01</sub>	LP <sub>11o</sub>	92%
LP <sub>01</sub>	LP <sub>11e</sub>	87%
LP <sub>01</sub>	LP <sub>21</sub>	82.5%

Input Mode	Converted Mode	Mode correlation
LP <sub>11o</sub>	LP <sub>01</sub>	91%
LP <sub>11e</sub>	LP <sub>01</sub>	86%
LP <sub>21</sub>	LP <sub>01</sub>	91%

### 4.3.2 Mode Conversion Efficiency

In this section mode conversion efficiency was investigated. Power of the mode before conversion and after conversion was measured. However it was not possible to calculate the efficiency as  $\frac{\text{output power}}{\text{input power}}$ . The figure 25 shows down converted LP<sub>01</sub> mode from LP<sub>11e</sub> mode (as seen in section 4.3.1.5). It can be seen even after mode conversion there is some non converted mode content. It is necessary to take this stray mode content into account before calculating final mode conversion efficiency.

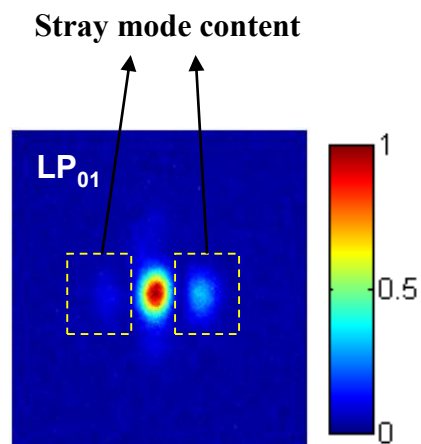


**Figure 25: Stray mode content left in LP<sub>01</sub> mode down converted from LP<sub>11e</sub> mode**



The mode conversion efficiency was calculated in steps mentioned below. Down conversion of  $LP_{01}$  mode from  $LP_{11e}$  mode is used as an example for better explanation of steps.

Step 1: Measurement of power before and after mode conversion

Power was measured before and after mode conversion. Power before mode conversion was termed as *input power* and power after mode conversion is termed as *output power*.

Step 2: Recording the far field image and subtracting background

Far field image of the mode as well as image of the background (without any input) was recorded and stored on computer in form of weighted matrix as explained earlier. The background was then subtracted from far field of the mode. This made sure that any spurious light recorded was cancelled out.

Step 3: Calculation of stray mode power

The output power corresponds to whole image and image is recorded in form of a matrix. Weight of each matrix element depends on intensity of corresponding pixel, hence the sum of all elements of the image matrix must be proportional to total output power.

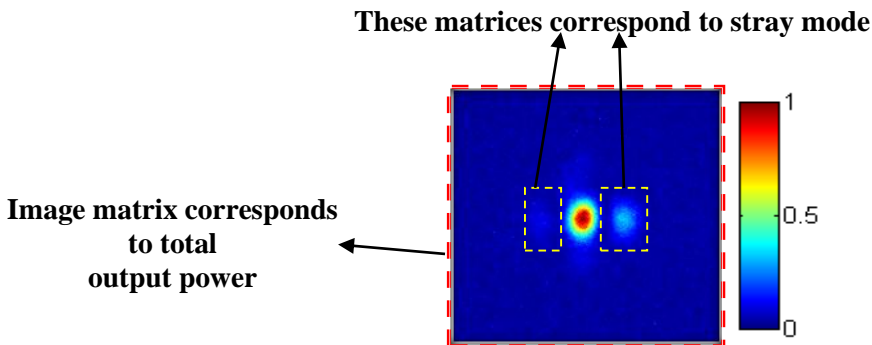


**Figure 26: Calculation of stray mode power**

Similarly sum of all matrix elements corresponding to pixels where stray mode is present must be proportional to stray mode power.

Now if we say, sum of all elements of image matrix is  $S_i$  and sum of matrix elements corresponding to stray mode content is  $S_s$ .

$$S_i \propto \text{Total output power} \quad (14)$$

$$S_s \propto \text{stray mode power} \quad (15)$$

$$\therefore \text{stray mode power} = \frac{\text{Total output power} \times S_s}{S_i} \quad (16)$$

Using MATLAB we can calculate values of  $S_i$  and  $S_s$ . For the example used here  $S_i = 155$ ,  $S_s = 788$  and *Total output power* = 67  $\mu\text{w}$  (from experiment). Using these values in equation 16, we get *stray mode power* = 13.17  $\mu\text{w}$ .

### Step 3: Calculation of mode conversion efficiency

The stray mode power was then subtracted from total output power to get power of converted mode. Using obtained values *power of converted mode* = 53.83  $\mu\text{w}$ . For input power of 78  $\mu\text{w}$  the mode conversion efficiency obtained was

$$\text{Mode conversion efficiency} = \frac{53.83}{78} \times 100 = 69\% \quad (17)$$

Using these steps, mode conversion efficiency for all converted modes were calculated. Theoretical mode conversion efficiency for a few conversions were calculated by Segal, M. et. al using model explained in section 2.1 [32]. The experimental and theoretical results are tabulated in table 3.

**Table 3: Mode conversion efficiencies of converted modes**

<b>Input Mode</b>	<b>Converted Mode</b>	<b>Mode Conversion Efficiency (Theoretical)</b>	<b>Mode Conversion Efficiency (Experimental)</b>
LP <sub>01</sub>	LP <sub>11o</sub>	~72%	70%
LP <sub>01</sub>	LP <sub>11e</sub>	~72%	69%
LP <sub>01</sub>	LP <sub>21</sub>	~65%	67%
LP <sub>11o</sub>	LP <sub>01</sub>	-	68%
LP <sub>11e</sub>	LP <sub>01</sub>	-	71%
LP <sub>21</sub>	LP <sub>01</sub>	~65%	62%

From the obtained results it was shown that high mode correlation up to 92% was achieved. Mode conversion efficiencies up to 71% were achieved with experimental results showing agreement with theoretical calculations.

## CHAPTER 5. SUMMARY, CONCLUSION AND OUTLOOK

In this investigation, it was successfully demonstrated that HPM can be used to convert LP fiber modes. In first experiment HPM was tested to operate at three different wavelengths 638 nm, 976 nm and 1076 nm. At these three wavelengths LP<sub>01</sub> mode was up converted in LP<sub>21</sub> mode. The experiments proved that the mask can be operated over a broad range of wavelengths. It was also shown that the HPM has high angular selectivity.

Second experiment investigated LP mode conversion using HPM at 1064 nm. LP modes were generated using a SLM. LP<sub>01</sub> mode was up converted in higher order LP<sub>11e</sub>, LP<sub>11o</sub> and LP<sub>21</sub> modes as well as LP<sub>11e</sub>, LP<sub>11o</sub> and LP<sub>21</sub> modes were down converted in LP<sub>01</sub> mode. High mode correlation factors up to 92% were obtained. The mode conversion efficiencies obtained were up to 71% and were in agreement with theoretical calculations.

The HPM has several promising applications in beam cleaning, spectral beam combing as well as mode multiplexing. HPM can also be implemented for power scaling of higher-order mode fiber lasers and amplifiers by combining mode conversion and beam combining.

The outlook of this project can include further analysis of mode purity with techniques like S<sup>2</sup> imaging and development of new HPM to convert various sets of modes for example, Bessel beams as non-diffracting large mode area beams. With development of PTR fiber and successful inscription of Bragg gratings in the fiber [33], an effort can be made to investigate the possibility of recording a mode converting device in a PTR optical fiber to create an all fiber monolithic system.

## **APPENDIX. ENCODING LP MODES ON SLM**

LP modes were calculated using FIMMWAVE. These modes were then extracted and encoded on SLM using MATLAB in following steps [34].

### **Step 1: Extracting the mode from FIMMWAVE**

First of all the resolution of FIMMWAVE was set to  $512 \times 512$ . This corresponds to the display of SLM ( $512 \times 512$  pixels). After a mode is calculated in FIMMWAVE, the corresponding data of the mode is extracted using MATLAB. This data is then normalized and saved in form of a 2D vector with all spatial components. A figure is then created to verify field amplitude, phase and intensity of extracted mode as shown in figure 27.

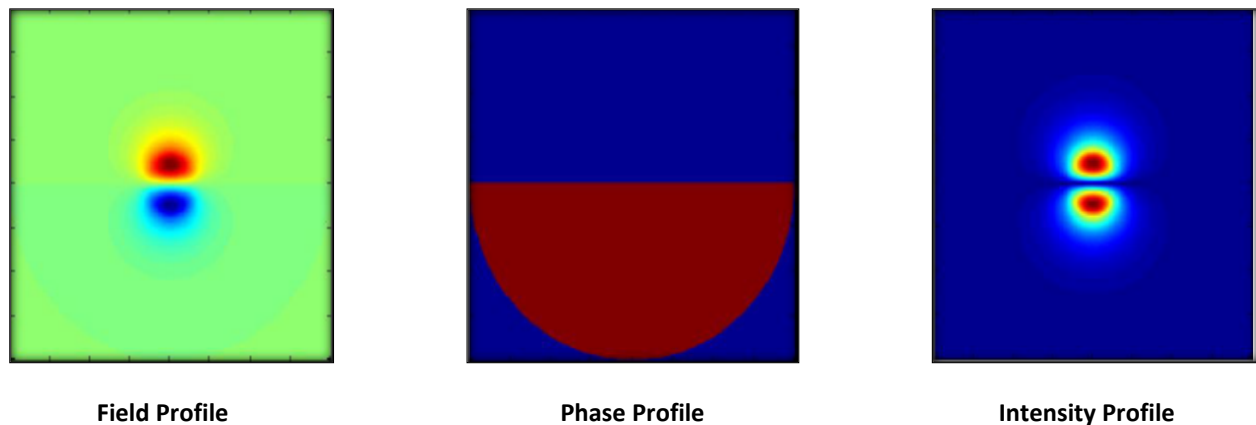


**Figure 27: Field, Phase and Intensity profiles of extracted mode**

Similarly other modes were extracted. All the extracted modes were then stored in a directory under numbered name.

### **Step 2: Storing all the modal fields in one 3D matrix**

Once modes were stored in a directory, they were then stored in form of a 3D matrix. The three dimensions are X, Y and Mode number. This step makes sure that there is no need to go back

to FIMMWAVE after modes are stored matrix form and this matrix of stored modes can be used for different applications.

### **Step 3: Encoding mode on SLM**

For this step SLM was connected with a HDMI or a DVI port to a computer. The connected SLM now acts as an extended display of the computer. MATLAB was then used to encode the mode using modelling technique reported by Arizon, V. et. al [31] (as explained earlier). This encoded mode was then displayed on SLM (acting as extended display). The encoded field in greyscale is shown in figure 28 (a), the corresponding intensity profile is shown in figure 28 (b).

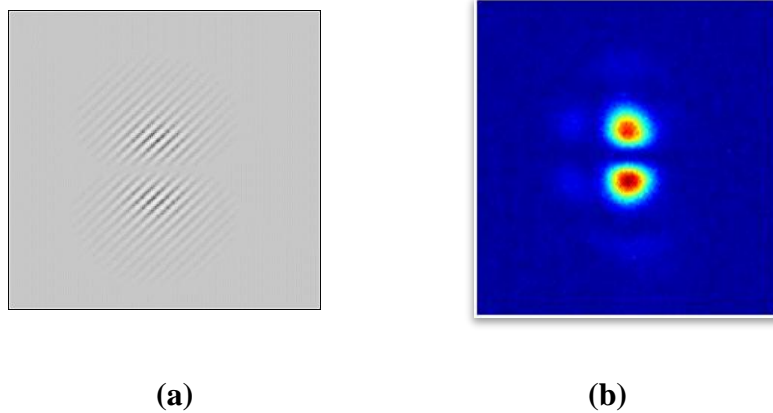


**Figure 28: (a) Field profile encoded on SLM (b) Corresponding intensity profile**

## REFERENCES

- [1] C. Jauregui, J. Limpert, and A. Tünnermann, “High-power fibre lasers,” *Nat. Photonics*, vol. 7, no. 11, pp. 861–867, Oct. 2013.
- [2] D. Gloge, “Optical fibres for communication,” *Appl. Opt.*, vol. 13, pp. 249–254, 1974.
- [3] D. J. Richardson, J. Nilsson, and W. a. Clarkson, “High power fiber lasers: current status and future perspectives,” *J. Opt. Soc. Am. B*, vol. 27, no. 11, p. B63, Oct. 2010.
- [4] A. W. Snyder, *Optical Waveguide Theory*. Springer, 1983.
- [5] S. B. Poole, D. N. Payne, and M. E. Fermann, “Fabrication of low-loss optical fibres containing rare-earth ions,” *Electron. Lett.*, vol. 21, no. 17, pp. 737–738, 1985.
- [6] J. W. Dawson, M. J. Messerly, R. J. Beach, M. Y. Shverdin, E. a Stappaerts, A. K. Sridharan, P. H. Pax, J. E. Heebner, C. W. Siders, and C. P. J. Barty, “Analysis of the scalability of diffraction-limited fiber lasers and amplifiers to high average power,” *Opt. Express*, vol. 16, no. 17, pp. 13240–66, Aug. 2008.
- [7] B. Crosignani, “Self-phase modulation and modal noise in optical fibers,” *J. Opt. Soc. Am. A. Opt. Image Sci. Vis.*, no. 3, pp. 16–18, 1982.
- [8] A. Kobayakov, M. Sauer, and D. Chowdhury, “Stimulated Brillouin scattering in optical fibers,” *Adv. Opt. Photonics*, vol. 2, no. 1, p. 1, Dec. 2009.
- [9] R. G. Smith, “Optical power handling capacity of low loss optical fibres as determined by stimulated Raman and Brillouin scattering,” *Appl. Opt.*, vol. 11, no. 11, pp. 2489–2494, 1972.
- [10] P. LiKamWa, *Guided waves and optoelectronics*. CREOL, The College of Optics and Photonics, 2013.
- [11] C. Jauregui, T. Eidam, J. Limpert, and A. Tünnermann, “The impact of modal interference on the beam quality of high-power fiber amplifiers,” *Opt. Express*, vol. 19, no. 4, pp. 3258–71, Feb. 2011.
- [12] N. G. R. Broderick, H. L. Offerhaus, D. J. Richardson, R. a. Sammut, J. Caplen, and L. Dong, “Large Mode Area Fibers for High Power Applications,” *Opt. Fiber Technol.*, vol. 5, no. 2, pp. 185–196, Apr. 1999.
- [13] J. Limpert, T. Schreiber, S. Nolte, H. Zellmer, and A. Tünnermann, “High-power air-clad large-mode-area photonic crystal fiber laser,” vol. 11, no. 7, pp. 818–823, 2003.



- [14] J. C. Baggett, T. M. Monro, K. Furusawa, and D. J. Richardson, “Comparative study of large-mode holey and conventional fibers,” *Opt. Lett.*, vol. 26, no. 14, pp. 1045–7, Jul. 2001.
- [15] J. P. Koplow, D. a Kliner, and L. Goldberg, “Single-mode operation of a coiled multimode fiber amplifier.,” *Opt. Lett.*, vol. 25, no. 7, pp. 442–4, Apr. 2000.
- [16] B. Ward, C. Robin, and I. Dajani, “Origin of thermal modal instabilities in large mode area fiber amplifiers.,” *Opt. Express*, vol. 20, no. 10, pp. 11407–22, May 2012.
- [17] S. Ramachandran, J. W. Nicholson, S. Ghalmi, M. F. Yan, P. Wisk, E. Monberg, and F. V Dimarcello, “Light propagation with ultralarge modal areas in optical fibers.,” *Opt. Lett.*, vol. 31, no. 12, pp. 1797–9, Jun. 2006.
- [18] M. SeGall, I. Divliansky, C. Jollivet, A. Schülzgen, and L. Glebov, “Simultaneous laser beam combining and mode conversion using multiplexed volume phase elements,” *Proc. SPIE*, vol. 8960, p. 89601F, Mar. 2014.
- [19] M. SeGall, I. B. Divliansky, and L. Glebov, “Simultaneous laser mode conversion and beam combining using multiplexed volume phase elements,” *Adv. Solid-State Lasers Congr. Tech. Dig.*, p. AW2A.9, 2013.
- [20] R. Paschotta, “Encyclopedia of Laser Physics and Technology.” 2014.
- [21] J. T. Verdeyen, *Laser electronics*, 3rd ed. Prentice Hall, 1995.
- [22] M. SeGall, V. Rotar, J. Lumeau, S. Mokhov, B. Zeldovich, and L. B. Glebov, “Binary volume phase masks in photo-thermo-refractive glass.,” *Opt. Lett.*, vol. 37, no. 7, pp. 1190–2, Apr. 2012.
- [23] L. B. Glebov, V. I. Smirnov, C. M. Stickley, and I. V Ciapurin, “New approach to robust optics for HEL systems,” *Proc. SPIE*, vol. 4724, pp. 101–109, 2002.
- [24] H. KOGELNIK, “Coupled Wave Theory for Thick Hologram Gratings,” *Bell Syst. Tech. J.*, 1969.
- [25] J. Goodman, *Introduction to Fourier optics*. Roberts & Co Publishers, 2005.
- [26] J. A. Buck, *Fundamentals of Optical Fibers*. Hoboken, NJ, 2004.
- [27] M. R. Vastag, “Mode Field Diameter and Effective Area,” *White Pap. Corning*, pp. 3–4, 2001.

- [28] “Point Grey imaging systems - Grasshopper Express CCD - Technical details,” pp. 1–9, 2013.
- [29] E. G. van Putten, I. M. Vellekoop, and a P. Mosk, “Spatial amplitude and phase modulation using commercial twisted nematic LCDs.,” *Appl. Opt.*, vol. 47, no. 12, pp. 2076–81, Apr. 2008.
- [30] “Boulder Nonlinear Systems - Spatial Light Modulator Datasheet,” no. November, pp. 1–12, 2010.
- [31] V. Arrizón, U. Ruiz, R. Carrada, and L. a González, “Pixelated phase computer holograms for the accurate encoding of scalar complex fields.,” *J. Opt. Soc. Am. A. Opt. Image Sci. Vis.*, vol. 24, no. 11, pp. 3500–7, Nov. 2007.
- [32] M. SeGall, I. Divliansky, C. Jollivet, A. Schulzgen, and L. Glebov, “Holographically encoded phase masks: A method to extend phase mask capabilities beyond traditional limitations.”
- [33] P. Hofmann, R. Amezcua-correa, E. Antonio-lopez, D. Ott, M. Segall, I. Divliansky, J. Lumeau, L. Glebova, L. Glebov, N. Peyghambarian, and A. Schulzgen, “Strong Bragg Gratings in Highly Photosensitive Photo-Thermo-Refractive-Glass Optical Fiber,” *IEEE Photonics Technol. Lett.*, vol. 25, no. 1, pp. 25–28, 2013.
- [34] C. Jollivet, *Complex field encoding and beam modulation using spatial light modulator - User Application Notes*. Fiber Optics Lab, CREOL, UCF, 2013, pp. 1–11.